iScience

CellPress
OPEN ACCESS

Article

EP300 restores the glycolytic activity and anti-tumor function of CD8$^+$ cytotoxic T cells in nasopharyngeal carcinoma

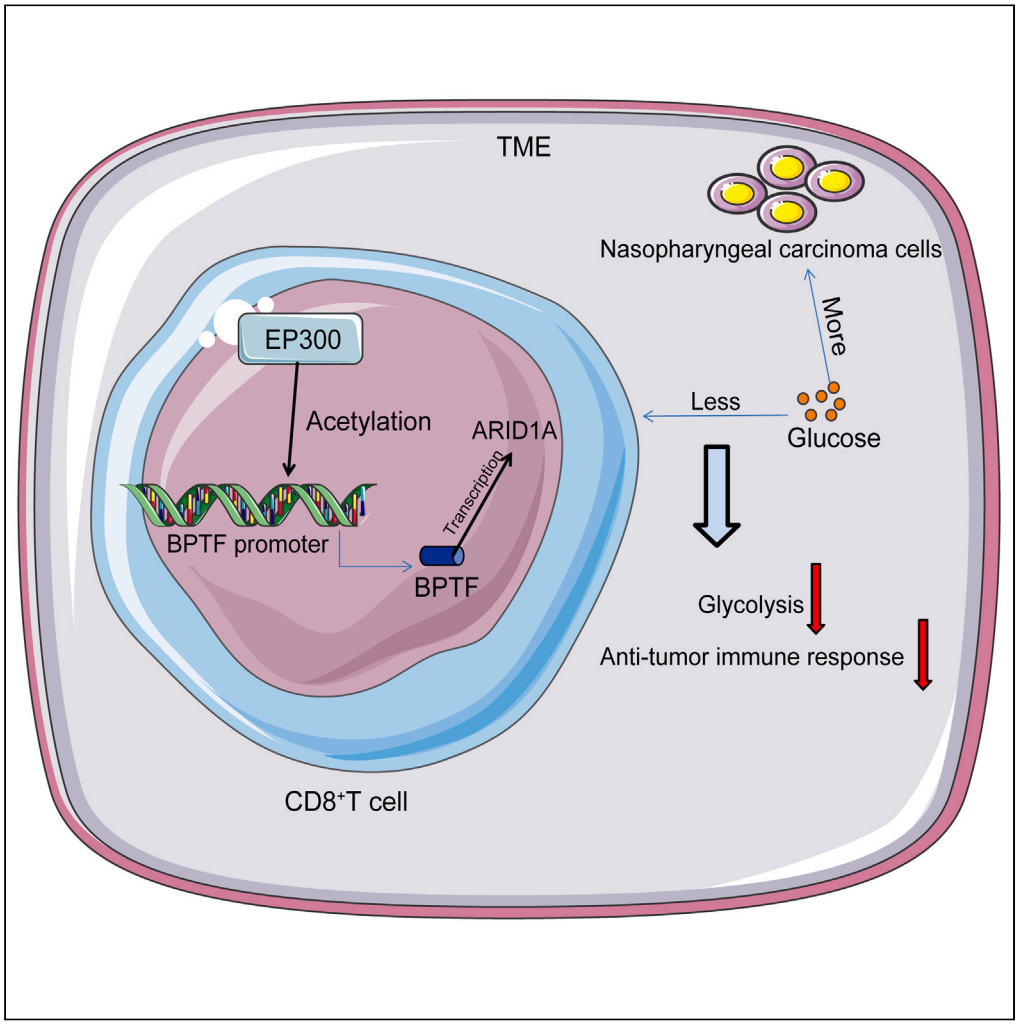

Zhixiu Xia, Xiaoxu Ding, Chao Ji, Dabo Zhou, Xun Sun, Tiancong Liu

tcliu@cmu.edu.cn

Highlights

Glucose metabolism of CD8$^+$ T cells is impaired in the TME of NPC

EP300 enhances glycolytic and anti-tumor immune activities of CD8$^+$ T cells

EP300 enhances BPTF expression through H3K27ac, and BPTF activates ARID1A transcription

Knockdown of BPTF or ARID1A counteracts the effects of EP300 on CD8$^+$ T cell activation

Xia et al., iScience 27, 108957
February 16, 2024
https://doi.org/10.1016/j.isci.2024.108957

iScience

CellPress
OPEN ACCESS

Article

EP300 restores the glycolytic activity and anti-tumor function of CD8$^+$ cytotoxic T cells in nasopharyngeal carcinoma

Zhixiu Xia,[1] Xiaoxu Ding,[2] Chao Ji,[3] Dabo Zhou,[4] Xun Sun,[5] and Tiancong Liu[2,6,*]

SUMMARY

Competition for glucose may metabolically limit T cells during cancer progression. This study shows that culturing in the condition medium (CM) of NPC c6661 cells restricted glycolytic and immune activities of CD8$^+$ T cells. These cells also exhibited limited tumor-eliminating effects in mouse xenograft tumor models. Glucose supplementation restored glycolysis and immune activity of CD8$^+$ T cells *in vitro* and *in vivo* by rescuing the expression of E1A binding protein p300 (EP300). EP300 upregulated bromodomain PHD finger transcription factor (BPTF) expression by catalyzing H3K27ac modification, and BPTF further activated AT-rich interaction domain 1A (ARID1A) transcription. Either BPTF or ARID1A knockdown in CD8$^+$ T cells reduced their glycolytic activity, decreased the secretion of cytotoxic molecules, and blocked the tumor-killing function in mice. Overall, this study demonstrates that EP300 restores the glycolytic and anti-tumor activities of CD8$^+$ T cells in the glucose restriction condition in NPC through the BPTF/ARID1A axis.

INTRODUCTION

Nasopharyngeal carcinoma (NPC) is among the most prevailing types of head and neck squamous carcinoma (HNSC).[1] According to the 2020 global cancer statistics, there were 133,354 new diagnoses and 80,008 deaths in that year.[2] NPC is characterized by skewed geographic distribution which is uncommon in most parts of the world but prevalent in southern China, southeast Asia, and northern Africa.[3] Current primary treatments including chemotherapy and radiotherapy have improved the overall survival of patients.[1]

While the presence of tumor infiltrating lymphocytes (TILs), especially CD8$^+$ T cells, is a positive prognostic marker in a variety of solid tumors, the T cells showed impaired function in eliminating cancer cells due to the immunosuppressive mechanisms in the tumor microenvironment (TME).[4] Therefore, immunotherapy targeting immune checkpoints such as programmed death-1 (PD-1) or programmed death-1 ligand has achieved breakthroughs for the management of metastatic or recurrent NPC diseases.[5] However, lymphocytes face metabolic challenges and adjust their metabolic activity to meet the increased metabolic demands of cell growth, proliferation, effector function, and adaption to changing environmental conditions.[6,7] Tumor cells also favor aerobic glycolysis even in the presence of completely functioning mitochondria to obtain energy for rapid and massive cell growth, proliferation, and maintenance.[8] Competition for glucose may metabolically limit T cells and restrict their immune activity during cancer progression.[9] Enhancing the glucose glycolytic activity of T cells is therefore a promising future direction for the management of solid tumors including NPC.

Histone acetylation represents one of the typical post-translational modifications that participate in various biological processes.[10] It refers to the addition of an acetyl group to histone lysine residues on histone tails by histone acetyltransferases (HATs).[11] Interestingly, treatment with acetate has been reported to increase the activity of glucose-restricted CD8$^+$ T cells and enhance the secretion of effector cytokine interferon gamma (IFN-γ) by increasing histone acetylation,[9] indicating the significant correlation of histone acetylation with the T cell reactivation. E1A binding protein p300 (EP300) is a member of the orphan family (CBP/EP300 and nuclear receptors) of HATs that manipulates transcription via chromatin remodeling and is crucial for cell proliferation and differentiation.[11,12] Of note, EP300 inhibition has been reported to be linked to impaired function of T cells.[13,14] Meanwhile, EP300 has been reported as an acetyltransferase for lysine 2-hydroxyisobutyrylation to mediate glycolysis in response to nutritional cues.[15] In this study, we aim to investigate the relevance of EP300 to the immune activity of CD8$^+$ T cells in glucose-restricted conditions.

[1]Colorectal Tumor Surgery Ward, Department of General Surgery, Shengjing Hospital of China Medical University, Shenyang 110004, Liaoning, P.R. China
[2]Department of Otorhinolaryngology-Head and Neck Surgery, Shengjing Hospital of China Medical University, Shenyang 110004, Liaoning, P.R. China
[3]Clinical Epidemiology Teaching and Research Section, Shengjing Hospital of China Medical University, Shenyang 110004, Liaoning, P.R. China
[4]Repair Teaching and Research Section, School and Hospital of Stomatology, China Medical University, Shenyang 110002, Liaoning, P.R. China
[5]Department of Immunology, College of Basic Medicine, China Medical University, Shenyang 110002, Liaoning, P.R. China
[6]Lead contact
*Correspondence: tcliu@cmu.edu.cn
https://doi.org/10.1016/j.isci.2024.108957

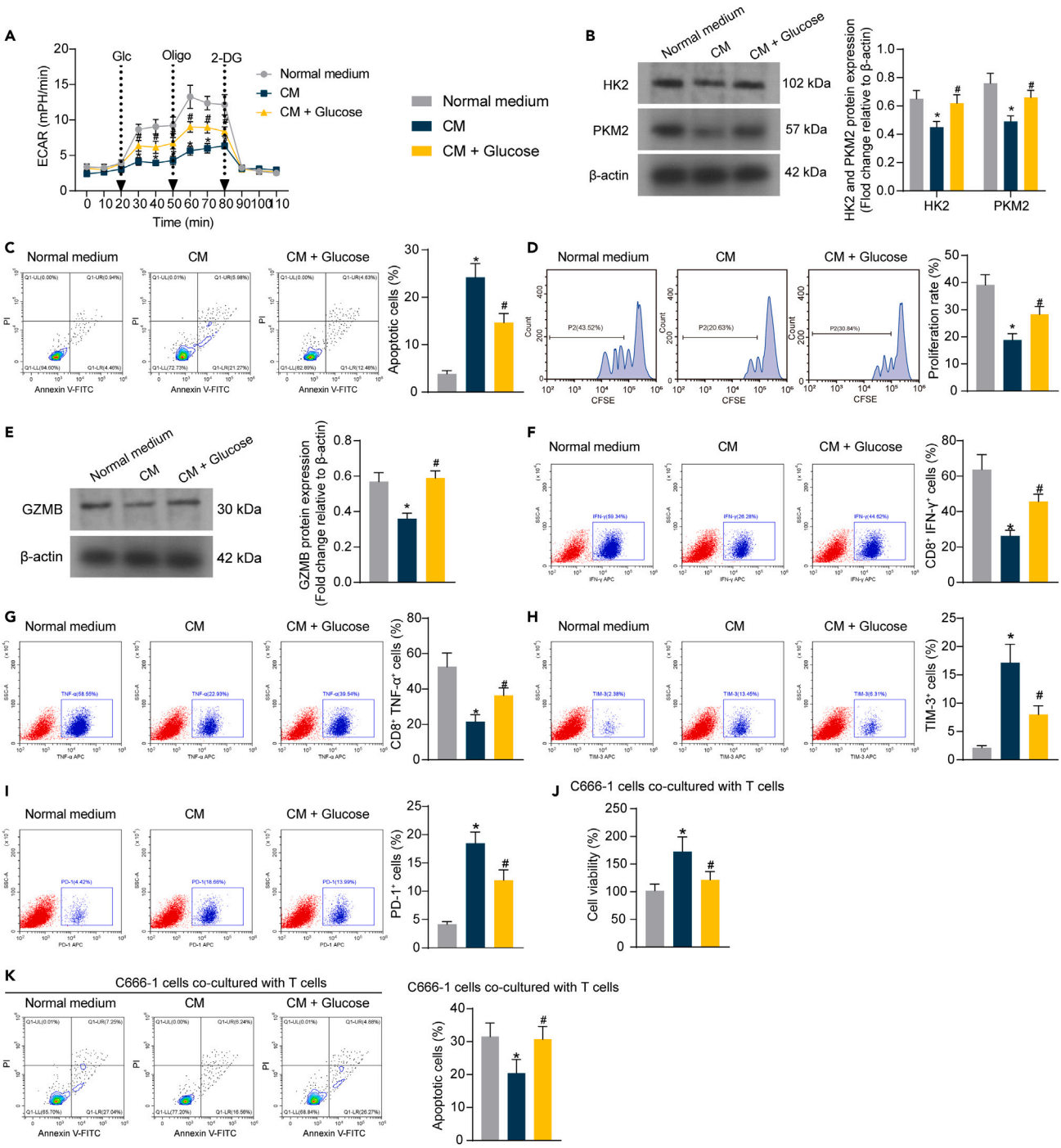

Figure 1. Glucose metabolism of CD8$^+$ T cells is impaired in the TME of NPC

(A) ECAR of the activated CD8$^+$ T cells after 24 h of culture in normal medium, CM of c6661 cells, and CM along with 2 mg/mL glucose, respectively.

(B) Protein levels of glycolysis-related HK2 and PKM2 in CD8$^+$ T cells detected by immunoblot analysis.

(C) Apoptosis of CD8$^+$ T cells determined by flow cytometry (FITC and PI labeling).

(D) Proliferation of CD8$^+$ T cells determined by flow cytometry (CFSE labeling).

(E) Protein level of the cytotoxic marker GZMB in CD8$^+$ T cells detected by immunoblot analysis.

(F and G) Proportions of IFN-γ$^+$ (F) and TNF-α$^+$ (G) CD8$^+$ T cells analyzed by flow cytometry.

(H and I) Proportions of TIM-3$^+$ (E) and PD-1$^+$ (F) CD8$^+$ T cells analyzed by flow cytometry.

Figure 1. *Continued*

(J) Viability of C666-1 cells after a 10-h direct co-culture with differentially treated CD8$^+$ T cells determined using CCK-8 assay.

(K) Apoptosis of C666-1 cells after a 10-h direct co-culture with differentially treated CD8$^+$ T cells determined by flow cytometry (FITC and PI labeling).

Differences were compared by one-way (C–K) or two-way (A and B) ANOVA. * vs. Normal medium; # vs. CM. *#p < 0.05. Three biological replicates were performed. The error bar denotes the standard deviation.

With the aid of advanced web-based bioinformatics tools, we obtained bromodomain PHD finger transcription factor (BPTF) as a candidate target of EP300 and AT-rich interaction domain 1A (ARID1A) a promising target of BPTF. BPTF is the largest subunit of nucleosome remodeling factor whose depletion in conditional mouse mutants impaired the maturation of thymocytes.[16] Likewise, ARID1A has been reported to promote the development of thymocytes.[17] However, the functions of BPTF and ARID1A in the activity of CD8$^+$ T cells in TME remain unclear. Collectively, this study was performed to examine the interactions between EP300, BPTF, and ARID1A and their functions in the regulation of glycolytic and immune activities of CD8$^+$ T cells in the TME of NPC.

RESULTS

Glucose metabolism of CD8$^+$ T cells is impaired in the tumor microenvironment of nasopharyngeal carcinoma

Restricted access to nutrients such as glucose may metabolically limit T cells and reduce their responsiveness during cancer progression.[7] To examine the glucose metabolism level and activity of CD8$^+$ T cells in the TME of NPC, we incubated activated CD8$^+$ T cells in normal medium, conditioned medium (CM) of c6661 cells, and CM added with 2 mg/mL glucose, respectively. Compared to the CD8$^+$ T cells cultured in normal medium, those cultured in CM showed significantly decreased extracellular acidification rate (ECAR), and the addition of glucose in CM partly restored the ECAR of the CD8$^+$ T cells (Figure 1A). The immunoblot analysis revealed that the CD8$^+$ T cells showed decreased levels of glycolysis-related proteins HK2 and PKM2 in the mimicked NPC TME *in vitro*. Still, the supplementation of glucose rescued the HK2 and PKM2 protein levels in the CD8$^+$ T cells (Figure 1B). The flow cytometry results showed that the *in vitro* apoptosis of CD8$^+$ T cells was increased when they were incubated in the CM but alleviated after the addition of glucose (Figure 1C). By contrast, the proliferation of CD8$^+$ T cells was decreased in the CM but rescued after glucose supplementation (Figure 1D). CD8$^+$ T cells cultured in CM expressed reduced protein level of the cytotoxic molecule granzyme B (GZMB), which was restored by the addition of glucose (Figure 1E). Meanwhile, in the mimicked TME, the proportions of IFN-γ^+ and tumor necrosis factor alpha (TNF-α)$^+$ CD8$^+$ T cells were substantially reduced, which were rescued by the supplementation of glucose (Figures 1F and 1G). The flow cytometric analysis also showed that the proportions of TIM3$^+$ and PD-1$^+$ CD8$^+$ T cells were significantly increased upon CM stimulation but restored after glucose supplementation as well (Figures 1H and 1I), indicating increased T cell exhaustion. To further examine the cytotoxicity of T cells, the differentially treated CD8$^+$ T cells were co-cultured with C666-1 cells in single wells of six-well plates. Notably, the CM-stimulated T cells showed significantly reduced cytotoxicity, as manifested by increased viability while decreased apoptosis of C666-1 cells after co-culture. Supplementing glucose significantly reversed the reduction in T cell cytotoxicity (Figures 1J and 1K). This body of evidence indicates that the anti-tumor activity of CD8$^+$ T cells is significantly reduced in the CM of NPC cells, which can be restored upon glucose supplementation.

E1A binding protein p300 enhances the glucose metabolic activity of CD8$^+$ T cells

The increase in histone acetylation has been reportedly linked to increased function of effector T cells under glucose restriction.[9] Among the HATs, EP300 has been reported to have specific links to the activity and function of T cells.[13,14] This attracted our interests to detect if EP300 showed any alteration during the glucose metabolic disorders of CD8$^+$ T cells. Indeed, the immunoblot analysis revealed that the protein level of EP300 in CD8$^+$ T cells was substantially reduced when they were cultured in the CM but then restored after the glucose addition (Figure 2A). To further explore the possible role of EP300 in regulating the glucose metabolic activity of the CD8$^+$ T cells, lentivirus (LV)-carried overexpression plasmid of EP300 (oe-EP300) or the negative control (oe-NC) was administered in the CD8$^+$ T cells. The successful EP300 protein elevation was detected by immunoblot analysis (Figure 2B). These cells were incubated in the CM. It was found that the ECAR of cells and the HK2 and PKM2 protein levels in cells were significantly increased after EP300 overexpression (Figures 2C and 2D). The flow cytometry showed that the apoptosis of activated CD8$^+$ T cells was decreased (Figure 2E), and the positive immunofluorescence staining of the proliferation marker protein Ki67 was elevated upon EP300 overexpression (Figure 2F). The CFSE staining validated an increase in CD8$^+$ T cell proliferation induced by oe-EP300 as well (Figure 2G). In addition, the EP300 overexpression also elevated the protein level of GZMB in the CD8$^+$ T cells (Figure 2H) and increased the proportions of IFN-γ^+ and TNF-α^+ cells (Figures 2I and 2J).

E1A binding protein p300 overexpression strengthens the anti-tumor effect of active CD8$^+$ T cells

The anti-tumor effect of active CD8$^+$ T cells was examined *in vivo*. The c666-1 cells were injected into mice subcutaneously to induce xenograft tumors, followed by the injection of PBS or activated CD8$^+$ T cells (Figure 3A). Not surprisingly, the CD8$^+$ T cells significantly slowed down the growth rate of the subcutaneous xenograft tumors in mice. However, the tumor-killing effect of CD8$^+$ T cells was weakened upon CM stimulation but rescued by further upregulation of EP300 (Figure 3B). The tumor weight showed a similar trend with the volume change in mice (Figure 3C). After animal euthanasia, the tumor tissues were collected. The subsequent flow cytometry revealed that the proportion of active CD8$^+$ T cells in the xenograft tissues was decreased in the setting of CM stimulation but rescued by artificial EP300 upregulation (Figure 3D). Moreover, the contents of IFN-γ, TNF-α, and GZMB in the tumors were reduced when the CD8$^+$ T cells were stimulated by CM but enhanced by EP300 upregulation (Figure 3E). Similarly, the protein levels of HK2 and PKM2 in the tumor tissues were repressed by CM but restored by EP300 as well (Figure 3F).

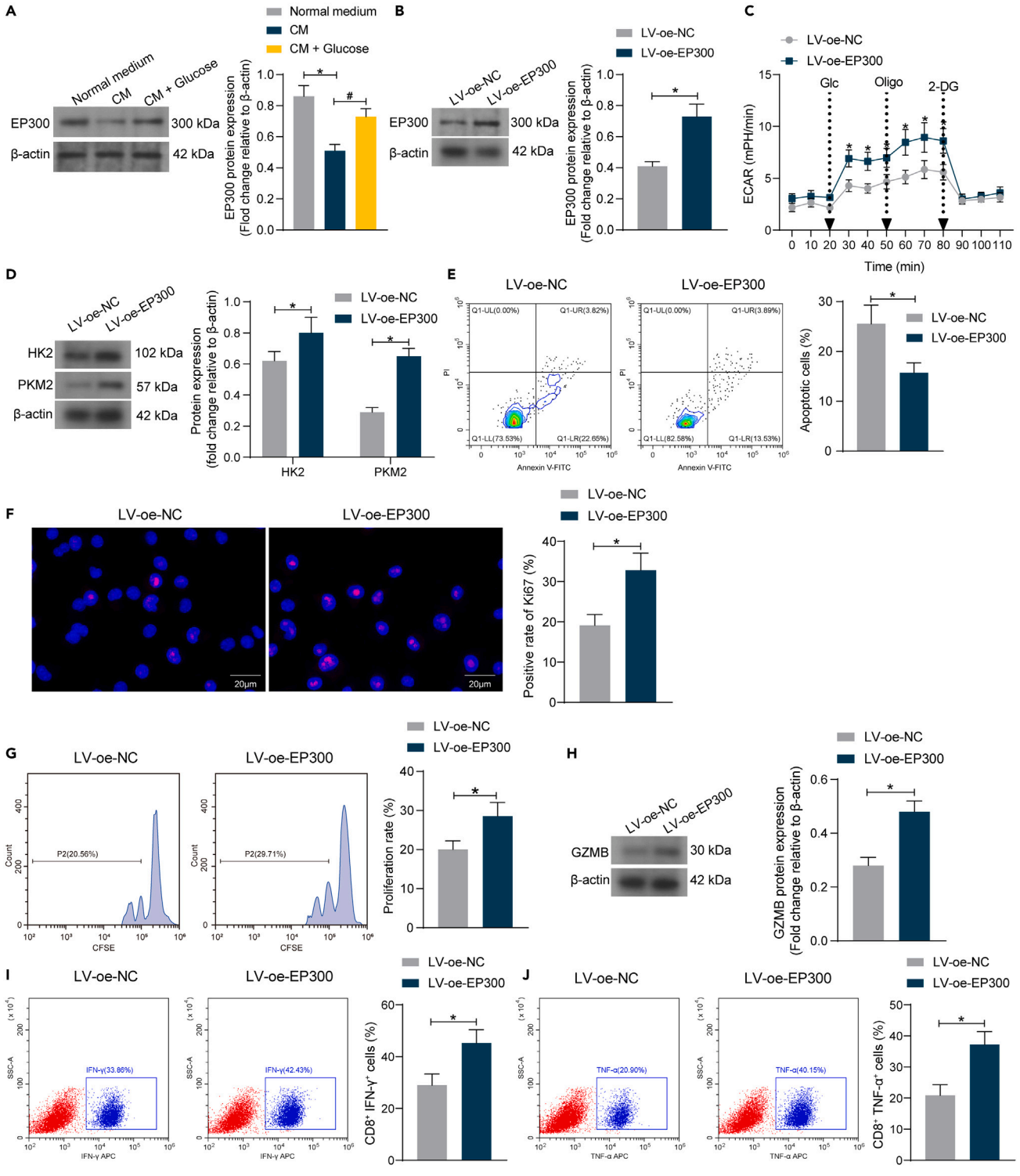

Figure 2. EP300 enhances the glucose metabolic activity of CD8⁺ T cells

(A) Protein level of EP300 in activated CD8⁺ T cells after 24 h of culture in normal medium, CM of c6661 cells, and CM containing 2 mg/mL glucose, respectively.

(B) Protein level of EP300 in CD8⁺ T cells after LV-oe-EP300 or LV-oe-NC administration determined by immunoblot analysis.

(C) ECAR of CD8⁺ T cells after EP300 overexpression.

(D) Protein levels of glycolysis-related HK2 and PKM2 in CD8⁺ T cells detected by immunoblot analysis.

(E) Apoptosis of CD8⁺ T cells determined by flow cytometry (FITC and PI labeling).

Figure 2. *Continued*

(F) Expression of the proliferation marker Ki67 in $CD8^+$ T cells determined by immunofluorescence staining.

(G) Proliferation of $CD8^+$ T cells determined by flow cytometry (CFSE labeling).

(H) Protein level of the cytotoxic marker GZMB in $CD8^+$ T cells detected by immunoblot analysis;

(I and J) Proportions of IFN-γ^+ (I) and TNF-α^+ (J) $CD8^+$ T cells analyzed by flow cytometer.

Differences were compared by the unpaired *t* test (B and E–J), one-way (A), or two-way (C and D) ANOVA. *#$p < 0.05$. Three biological replicates were performed. The error bar denotes the standard deviation. In panel F, scale bar = 20 μm.

E1A binding protein p300 enhances bromodomain PHD finger transcription factor expression in $CD8^+$ T cells via acetylation modification

To unravel more molecules regulated by EP300, we predicted genes showing positive correlation with EP300 in HNSC in UALCAN (http://ualcan.path.uab.edu/index.html) (Figure 4A). The top 100 genes (ranked in the order of correlation coefficient) were collected to establish a protein-protein-interaction (PPI) network. We observed that BPTF showed outstanding interaction effects in the network (Figure 4B). BPTF is crucial for the maturation of thymocytes.[16] Thereafter, we examined by quantitative polymerase chain reaction (qPCR) analysis that the BPTF expression in $CD8^+$ T cells was significantly reduced after 24 h of CM stimulation and restored after the supplementation of glucose (Figure 4C). In the UCSC database (http://genome.ucsc.edu/index.html), we obtained that the EP300 have binding peaks at the BPTF promoter, and there exists significant acetylation on histone H3, lysine-27 (H3K27ac) at the BPTF promoter (Figure 4D). Considering EP300 as a typical HAT catalyzing H3K27ac, we speculated that EP300 increases H3K27ac at the BPTF promoter to enhance BPTF expression. Immunoblot analysis also identified a decrease in H3K27ac protein level in $CD8^+$ T cells cultured in CM and a subsequent H3K27ac restoration following the glucose supplementation (Figure 4E). In $CD8^+$ T cells overexpressing EP300, increased BPTF mRNA (Figure 4F) and H3K27ac protein (Figure 4G) expression levels were detected. Through the chromatin immunoprecipitation (ChIP)-qPCR assay, abundant BPTF promoter fragments were detected in the immune complexes precipitated by EP300 and H3K27ac antibodies (Figure 4H). These results suggest that EP300 promotes BPTF expression in $CD8^+$ T cells via acetylation modification.

Knockdown of bromodomain PHD finger transcription factor counteracts the function of E1A binding protein p300 and reduces the activity of $CD8^+$ T cells

Knockdown of BPTF was further induced in $CD8^+$ T cells with EP300 overexpression, and the successful knockdown was validated by qPCR analysis (Figure 5A). The BPTF knockdown significantly reduced ECAR of $CD8^+$ T cells (Figure 5B) and reduced the protein levels of HK2 and PKM2 (Figure 5C). The flow cytometry and immunofluorescence staining revealed that the apoptosis of $CD8^+$ T cells was increased (Figure 5D) but the positive staining rate of Ki67 (Figure 5E) and cell proliferation were reduced (Figure 5F) after BPTF knockdown. Meanwhile, the LV-sh-BPTF reduced the protein level of GZMB in $CD8^+$ T cells (Figure 5G) and decreased the proportions of IFN-γ^+ and TNF-α^+ cells (Figures 5H and 5I).

Bromodomain PHD finger transcription factor promotes AT-rich interaction domain 1A transcription

According to the hTFtarget system (http://bioinfo.life.hust.edu.cn/hTFtarget#!/), BPTF is suggested to function as a transcription factor manipulating the expression of a variety of downstream genes. Therefore, we predicted genes showing positive correlation with BPTF in the UALCAN database (Figure 6A) and obtained the top 100 genes (ranked in the order of correlation coefficient) to establish the PPI network (Figure 6B). ARID1A was found to have significant interactions with other molecules, and it has been reported to promote the thymocyte development,[17] indicating its possible role in T cell function. Thereafter, we obtained the putative binding relationship between BPTF and ARID1A in the UCSC database (Figure 6C). Meanwhile, ARID1A was predicted as a downstream target of BPTF in the hTFtarget system (http://bioinfo.life.hust.edu.cn/hTFtarget#!/) (Figure 6D). In $CD8^+$ T cells, the ARID1A expression was decreased by BPTF silencing (Figure 6E). Downregulation of ARID1A was also detected in $CD8^+$ T cells cultured in CM, and the expression was restored after glucose addition (Figure 6F). The direct binding of BPTF with ARID1A was then validated by ChIP-qPCR (Figure 6G). Moreover, we induced BPTF downregulation alone in $CD8^+$ T cells. In this setting, the ARID1A expression was decreased (Figure 6H). The dual luciferase reporter gene assay also revealed that the BPTF knockdown reduced the luciferase activity of the reporter containing the ARID1A promoter sequence (Figure 6I).

Knockdown of AT-rich interaction domain 1A affects the activity of $CD8^+$ T cells

Similarly, ARID1A downregulation was induced in EP300-overexpressing $CD8^+$ T cells using LV-sh-ARID1A, and the successful knockdown was validated by qPCR analysis again (Figure 7A). It was observed that the ARID1A downregulation decreased ECAR of $CD8^+$ T cells (Figure 7B) and reduced the levels of HK2 and PKM2 protein (Figure 7C). The apoptosis of $CD8^+$ T cells was induced (Figure 7D) while the expression of Ki67 (Figure 7E) and cell proliferation (Figure 7F) were decreased in this setting. Moreover, the ARID1A knockdown substantially decreased the protein level of GZMB in $CD8^+$ T cells (Figure 7G) as well as reduced the proportions of IFN-γ^+ and TNF-α^+ cells (Figures 7H and 7I).

Knockdown of bromodomain PHD finger transcription factor or AT-rich interaction domain 1A counteracts the effects of E1A binding protein p300-mediated $CD8^+$ T activity *in vivo*

The interactions and functions of EP300, BPTF, and ARID1A were validated *in vivo*. The c666-1 cells were injected into mice to induce subcutaneous xenograft tumors, followed by the injection of $CD8^+$ T cells infected with LV-oe-E300, LV-oe-E300 + sh-BPTF or

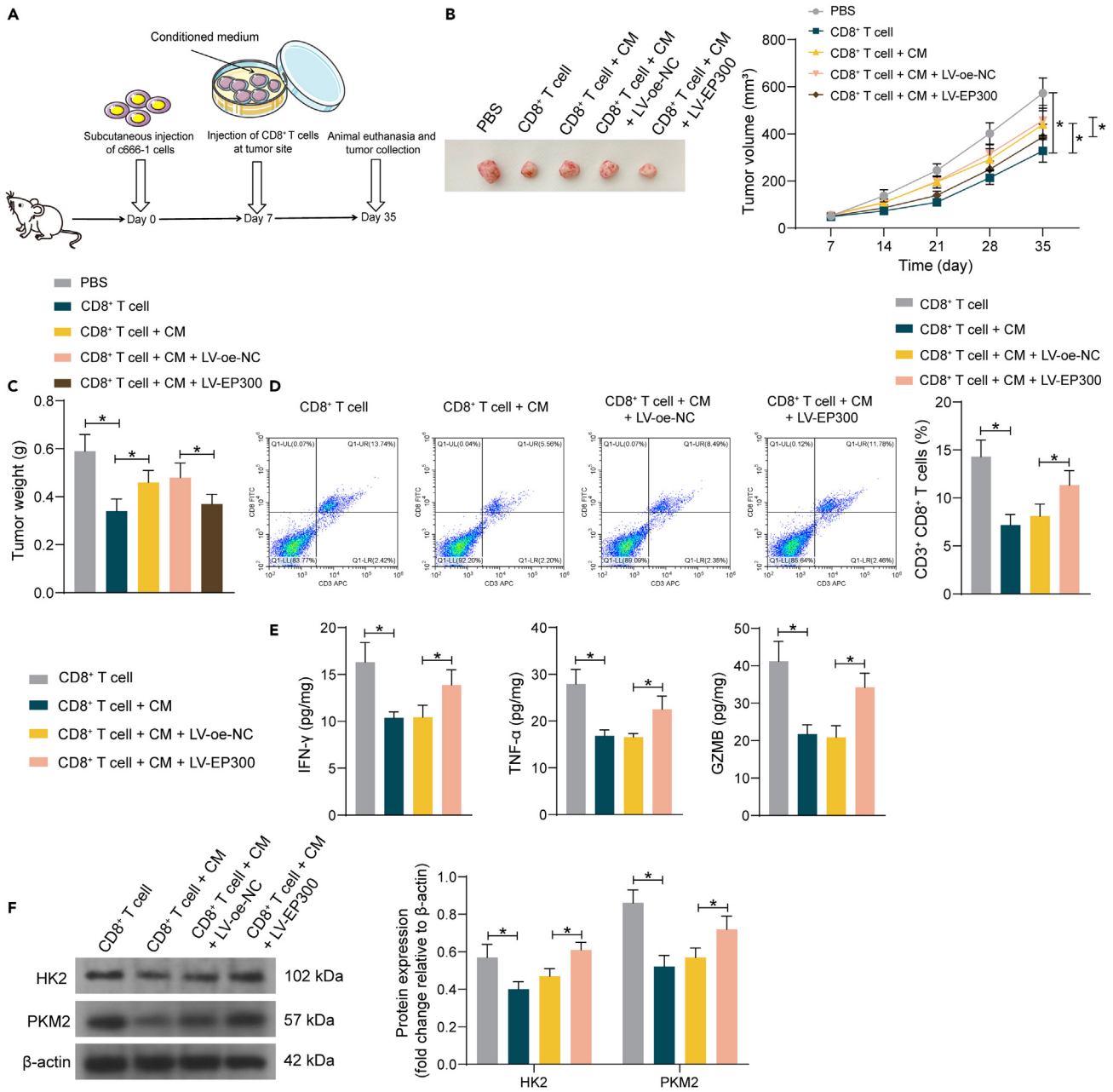

Figure 3. EP300 overexpression strengthens the anti-tumor effect of active CD8$^+$ T cells

(A) A diagram for the establishment of xenograft animal models.

(B) Volume change of the xenograft tumors in mice.

(C) Tumor weight in each group of mice on day 35.

(D) Proportion of active CD8$^+$ T cells in the single cell suspension of xenograft tumor tissues analyzed by flow cytometry.

(E) Contents of IFN-γ, TNF-α, and GZMB in xenograft tumor tissues determined using ELISA kits.

(F) Protein levels of HK2 and PKM2 in the CD8$^+$ T cells sorted from tumor tissues examined by immunoblot analysis.

Differences were compared by one-way (C–E) or two-way (B and F) ANOVA. *p < 0.05. For animal experiments, each group contained five mice. The error bar denotes the standard deviation.

LV-oe-E300 + sh-ARID1A. It was observed that the tumor-eliminating function of CD8$^+$ T cells was significantly weakened after BPTF or ARID1A knockdown (Figures 8A and 8B). Meanwhile, the administration of LV-sh-BPTF or LV-sh-ARID1A led to a substantial decline in the proportion of active CD8$^+$ T cells in the tumor tissues (Figure 8C), along with a reduction in the contents of IFN-γ, TNF-α and GZMB (Figure 8D). In the isolated CD8$^+$ T cells from tumor tissues, reduced protein levels of HK2 and PKM were detected as well (Figure 8E).

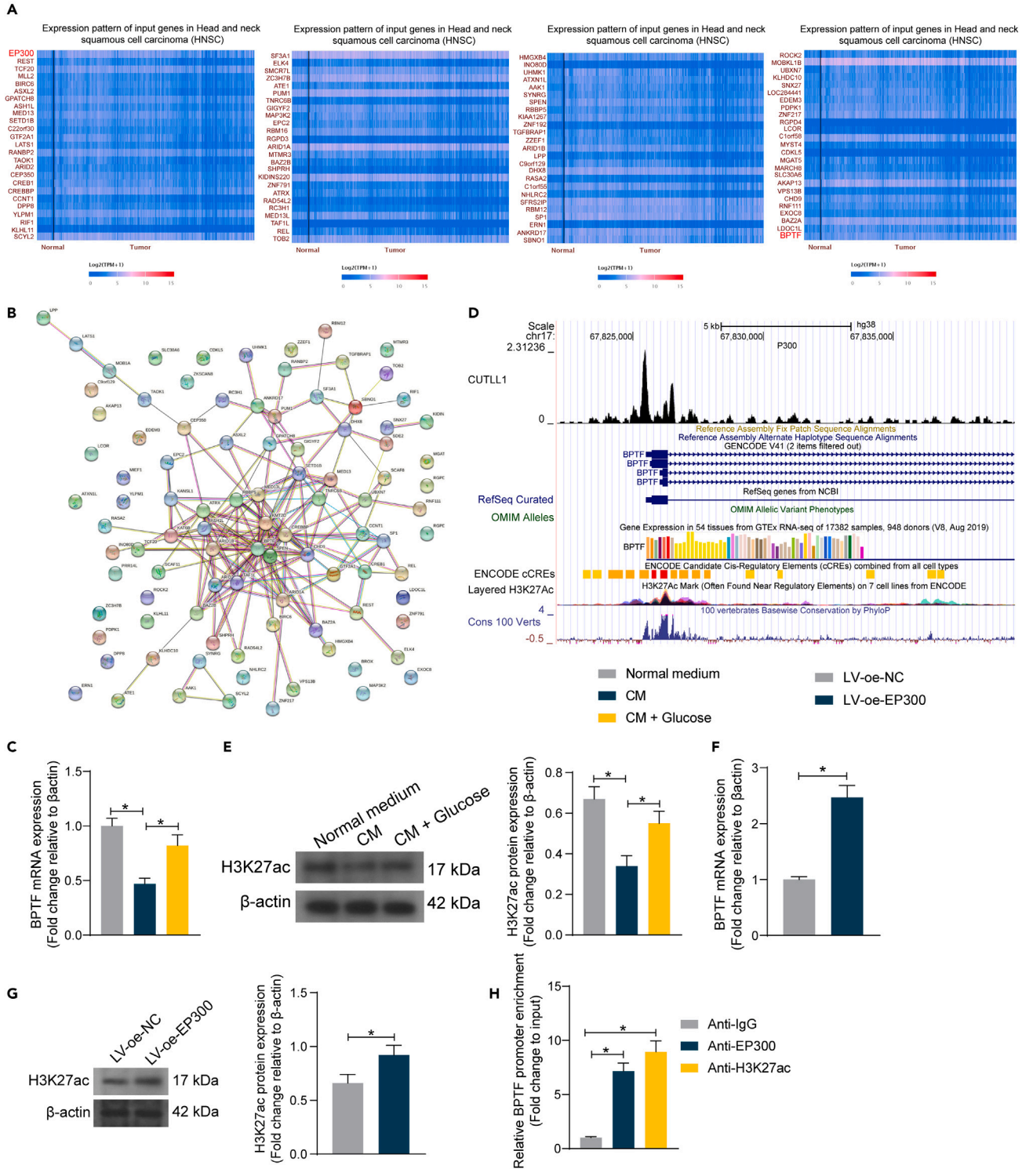

Figure 4. EP300 enhances BPTF expression in CD8$^+$ T cells via acetylation modification

(A) Top 100 genes (ranked by Pearson's correlation coefficient) showing positive correlation with EP300 in HNSC in UALCAN (on the left side of the image are listed the names of genes; the colors shown in the image represent the levels of gene expression, where the colors range from blue to red indicating low to high gene expression).

(B) A PPI network of the 100 genes established by the STRING system (https://string-db.org/).

(C) mRNA expression of BPTF in CD8$^+$ T cells after 24 h of culture in normal medium, CM, and CM containing 2 mg/mL glucose determined by qPCR analysis.

Figure 4. *Continued*

(D) Binding between EP300 and BPTF promoter predicted in the UCSC system.

(E) Protein level of H3K27ac in $CD8^+$ T cells after different treatments determined by immunoblot analysis.

(F) BPTF mRNA in $CD8^+$ T cells after EP300 overexpression determined by qPCR analysis.

(G) Protein level of H3K27ac in $CD8^+$ T cells after EP300 overexpression analyzed by immunoblot analysis.

(H) Abundance of BPTF promoter fragments in the complexes precipitated by EP300 and H3K27ac antibodies in the ChIP-qPCR assay.

Differences were compared by the unpaired *t* test (F and G) or one-way ANOVA (C, E, and H) ANOVA. *$p < 0.05$. Three biological replicates were performed. The error bar denotes the standard deviation.

DISCUSSION

Metabolic impairments of T cells including decline in glucose uptake and use, dysregulation of mitochondrial energetics, and the activation of anabolic pathways already develop during the first weeks of infection prior to the occurrence of a major loss in effector functions.[4] Restoration of the glycolytic activity of T cells is fundamental for their proliferation and maintenance, therefore fulfilling essential anti-tumor functions. In this study, we report that the EP300 downregulation is linked to the glucose metabolic impairment and functional loss of $CD8^+$ T cells in the TME of NPC. Artificial rescue of EP300 levels in $CD8^+$ T cells is hopeful to enhance their glycolytic and anti-tumor activities by augmenting the BPTF/ARID1A axis.

$CD8^+$ T cells are the major TILs capable of directly killing tumor cells.[18] First, we cultured $CD8^+$ T cells in the CM of c6661 cells to mimic the TME of NPC *in vitro*. The CM stimulation led to significantly decreased glycolytic and immune activities of $CD8^+$ T cells, as manifested by substantially reduced protein levels of HK2 and PKM2 and decreased the expression of cytotoxicity-related cytokines GZMB, IFN-γ, and TNF-α. We also found that the supplemental glucose in the CM restored the glycolytic and immune activities. Indeed, the importance of glucose for T cell responses has been demonstrated in a multitude of observational studies. Cham and colleagues demonstrated that the glucose-dependent metabolism is crucial of the maturation and activation of $CD8^+$ T cells, and the glucose deprivation rather than oxygen deprivation substantially suppressed the production of IFN-γ, upregulation of GZMB protein, and the cytolytic activity of the T cells.[19,20] Likewise, the surface trafficking of the glucose transporter Glut1 was critical for sustained T cell activation and the effector function.[21] Moreover, glucose consumption by tumors metabolically restricted T cells, and the administration of immune checkpoint blockade antibodies restored glucose levels in tumors, therefore enabling T cell glycolysis and IFN-γ production.[22] T cells extracted from fasting animals showed persistent metabolic and functional defects marked by decreased glucose uptake and reduced the production of inflammatory cytokines.[23] In this study, using xenograft mouse models, we confirmed that the tumor-eliminating role of the $CD8^+$ T cells was blocked upon CM stimulation but restored by glucose supplementation. Overall, our experimental results and the previous findings emphasize the importance of glucose supply and glycolysis for the activity of effector T cells.

The glucose uptake and aerobic glycolysis in activated T cells are highly orchestrated processes that are regulated both transcriptionally and post-transcriptionally.[6] We noticed that the CM stimulation significantly reduced the protein level of EP300 in the $CD8^+$ T cells, which was restored by glucose supplementation. Acetate-induced histone acetylation has been found to increase the secretion of IFN-γ in glucose-restricted $CD8^+$ T cells.[9] Moreover, EP300-mediated lysine 2-hydroxyisobutyrylation has been found to affect a multitude of glycolytic enzymes, consequently leading to glycolysis impairment and increased glucose depletion-induced cell death.[15] Upregulation of EP300 mediated by SET domain containing 5 increased nuclear accumulation of hypoxia-inducible factor 1α to enhance the glycolysis in breast cancer stem-like cells.[24] Moreover, EP300 expression has reportedly been positively correlated with the IFN-γ secretion in $CD8^+$ T cells in severe aplastic anemia.[25] In this study, we found that the artificial upregulation of EP300 in the $CD8^+$ T cells enhanced the glycolytic activity and promoted the secretion of GZMB, IFN-γ and TNF-α. Moreover, the $CD8^+$ T cells overexpressing EP300 showed significantly restored anti-tumor effect in mice with xenograft tumors. This compelling evidence suggests that the maintenance of EP300 level in the TME is hopeful to sustain the activity of effector T cells.

EP300 can regulate histone acetylation by catalyzing H3K27ac, a well-recognized marker for active enhancers and promoters, therefore activating the transcription of downstream targets.[20,26] By applying the UALCAN, STRING, and UCSC bioinformatics systems and performing ChIP-qPCR and luciferase assays, we obtained that EP300 activated BPTF transcription by catalyzing H3K27ac at the BPTF promoter. Moreover, ARID1A was confirmed as a candidate target of BPTF in a similarly manner. As a transcription factor, BPTF directly promoted ARID1A transcription instead. Both BPTF and ARID1A were downregulated in T cells upon CM stimulation but rescued after glucose supplementation or EP300 overexpression. BPTF is crucial for the maturation of thymocytes,[16] and it has been reported to be essential for the homeostasis and function of T cells.[27] Meanwhile, BPTF has been reported to play a pro-glycolytic role in cancers.[28,29] As for ARID1A, it has been reported to promote thymocyte development as well.[17] Similar trend has been demonstrated in a previous study by Audrey et al.[30] They found that the ARID1A deletion in early lymphoid progenitors in mice led to significant developmental arrest in early T cells and a substantial decline in the number of $CD4^+$ $CD8^+$ cells.[30] In patients with ovarian clear cell carcinoma, the downregulation of ARID1A was linked to reduced infiltration of $CD8^+$ T cells and poor survival.[31] Meanwhile, ARID1A mutation or alteration has reportedly been linked to reduced tumor infiltration, impaired IFN gene expression, limited chromatin accessibility to IFN-responsive genes, and poor tumor immunity.[32] In this study, we verified that either BPTF or ARID1A knockdown in $CD8^+$ T cells counteracted the function of EP300, reduced the glycolytic activity, decreased the secretion of cytotoxic molecules, and blocked the tumor-eliminating function in mice.

In conclusion, this study underscores the significance of EP300, an important HAT, in regulating the glycolytic and immune activities of cytotoxic $CD8^+$ T cells within the TME of NPC. The downregulation of EP300 is intricately linked to diminished glycolytic and immune functions in cytotoxic $CD8^+$ T cells. EP300 upregulation increases BPTF expression through H3K27ac modification. Subsequently, BPTF activates the transcription of ARID1A, thereby restoring glycolytic activity and anti-tumor immune function in $CD8^+$ T cells (Figure 9). Collectively,

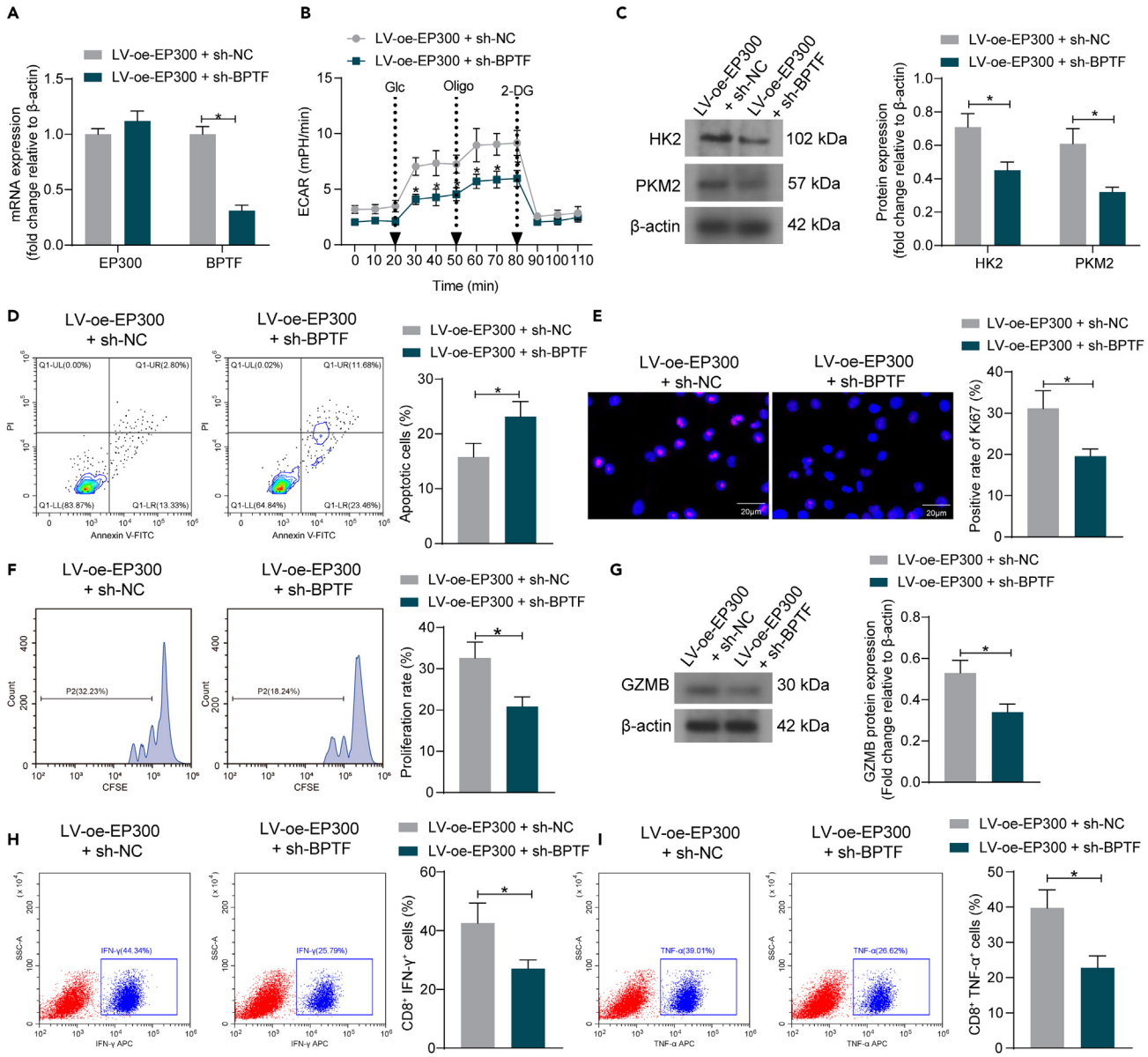

Figure 5. Knockdown of BPTF counteracts the function of EP300 and reduces the activity of CD8$^+$ T cells

(A) BPTF mRNA expression in CD8$^+$ T cells after LV-sh-BPTF infection detected by qPCR analysis.

(B) ECAR of the CD8$^+$ T cells after BPTF knockdown.

(C) Protein levels of HK2 and PKM2 in the CD8$^+$ T cells detected by immunoblot analysis.

(D) Apoptosis of the CD8$^+$ T cells determined by flow cytometry (FITC and PI labeling).

(E) Expression of the Ki67 in the CD8$^+$ T cells determined by immunofluorescence staining.

(F) Proliferation of CD8$^+$ T cells determined by flow cytometry (CFSE labeling).

(G) Protein level of GZMB in CD8$^+$ T cells detected by immunoblot analysis.

(H and I) Proportions of IFN-γ$^+$ (H) and TNF-α$^+$ (I) CD8$^+$ T cells analyzed by flow cytometer.

Differences were compared by the unpaired *t* test (D–I) or two-way (A–C) ANOVA. *p < 0.05. Three biological replicates were performed. The error bar denotes the standard deviation. In panel F, scale bar = 20 μm.

maintaining optimal levels of EP300/BPTF/ARID1A in the TME of NPC holds the potential to enhance T cell glycolysis and facilitate tumor elimination. It is worth mentioning that the study's focus on c6661 cells, which are EBV-positive, opens avenues for exploring targeted therapies. Specifically, existing evidence has demonstrated the effectiveness of CAR-T cells specifically targeting EBV antigen gp350 or LMP1 exerting pronounced anti-tumor effects.[33,34] In light of this, investigating the cytotoxic effects of EBV-specific CAR-T cells on c6661 cells in a glucose-limited microenvironment could significantly enhance the clinical relevance of this study. Unfortunately, this aspect was not

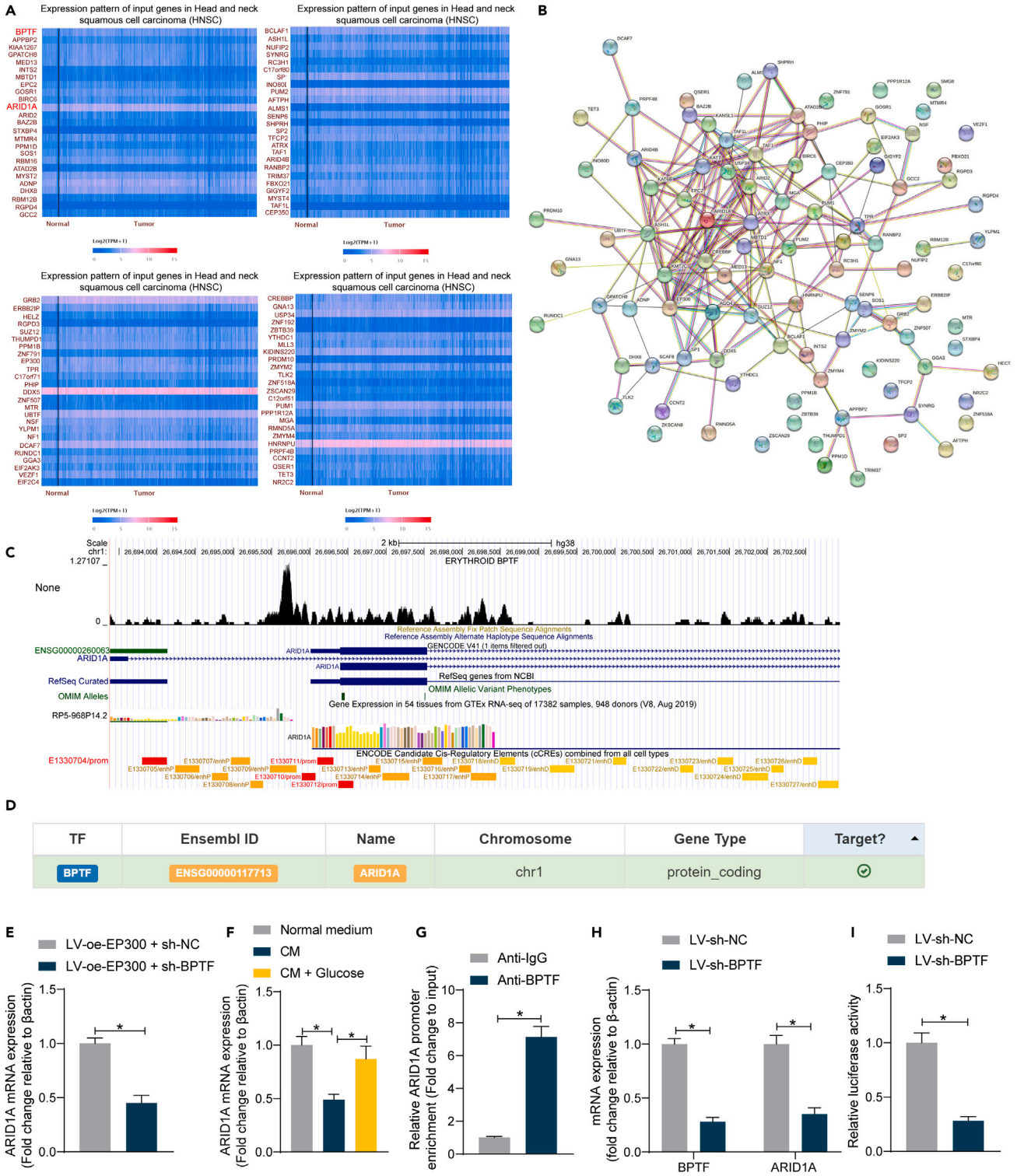

Figure 6. BPTF promotes ARID1A transcription

(A) Top 100 genes (ranked by Pearson's correlation coefficient) showing positive correlation with BPTF in HNSC in UALCAN (on the left side of the image are listed the names of genes; the colors shown in the image represent the levels of gene expression, where the colors range from blue to red indicating low to high gene expression).

Figure 6. *Continued*

(B) A PPI network of the 100 genes established by the STRING system.
(C) Binding peaks between BPTF and ARID1A promoter predicted in the UCSC system.
(D) Transcriptional regulation between BPTF and ARID1A predicted in the hTFtarget system.
(E) ARID1A mRNA in $CD8^+$ T cells after BPTF downregulation in the presence of EP300 overexpression determined by qPCR analysis.
(F) ARID1A mRNA expression in $CD8^+$ T cells after different stimulation/treatments determined by qPCR analysis.
(G) abundance of ARID1A promoter fragments in the complexes precipitated by BPTF antibody in the ChIP-qPCR assay.
(H) ARID1A mRNA in $CD8^+$ T cells after BPTF downregulation alone determined by qPCR analysis.
(I) binding between BPTF and the ARID1A promoter in $CD8^+$ T cells validated by luciferase assay.
Differences were compared by the unpaired *t* test (E and G), or by one-way ANOVA (F) or two-way (H) ANOVA. *$p < 0.05$. Three biological replicates were performed. The error bar denotes the standard deviation.

addressed in the current research due to technical and economic constraints. However, it remains a focal point for our future research endeavors, aiming to bridge this gap and further enrich the translational implications of our findings.

Limitations of the study

While our study identified the role of the EP300/BPTF/ARID1A axis in the glycolytic activity and anti-tumor effect of $CD8^+$ T cells on NPC cells both *in vitro* and *in vivo*, there are some limitations to our work. First, we could not analyze clinical samples due to the inadequate number of samples available for research, which may limit the clinical translational value of our study. Additionally, we selected EP300 as a primary subject for this research based on literature supporting the correlation between HATs, including EP300, with T cell function. However, due to funding limitations, we were unable to perform RNA or transcriptome sequencing analyses to validate the importance of EP300 in T cell dysfunction. We plan to address these limitations in future research.

STAR★METHODS

Detailed methods are provided in the online version of this paper and include the following:

- KEY RESOURCES TABLE
- RESOURCE AVAILABILITY
  - Lead contact
  - Materials availability
  - Data and code availability
- EXPERIMENTAL MODEL AND STUDY PARTICIPANT DETAILS
  - Xenograft mouse models
- METHOD DETAILS
  - Cells
  - Lentivirus infection
  - RNA extraction and quantification
  - Immunoblot analysis
  - Co-culture of T cells with C666-1 cells
  - CCK-8 method
  - Enzyme-linked immunosorbent assay (ELISA)
  - Flow cytometry
  - ECAR examination
  - Immunofluorescence staining
  - $CD8^+$ T cell proliferation examined using carboxyfluorescein diacetate succinimidyl ester (CFSE) staining
  - ChIP-qPCR
  - Dual luciferase reporter gene assay
- QUANTIFICATION AND STATISTICAL ANALYSIS

SUPPLEMENTAL INFORMATION

Supplemental information can be found online at https://doi.org/10.1016/j.isci.2024.108957.

ACKNOWLEDGMENTS

We thanks to the Doctoral Research Foundation Project of Liaoning Province (Grant No. 2022-BS-130), the Projects of Shenyang Science and Technology Bureau (grant no. 20-205-4-029) and the 345 Talent Project of Shengjing Hospital of China Medical University for the funding support.

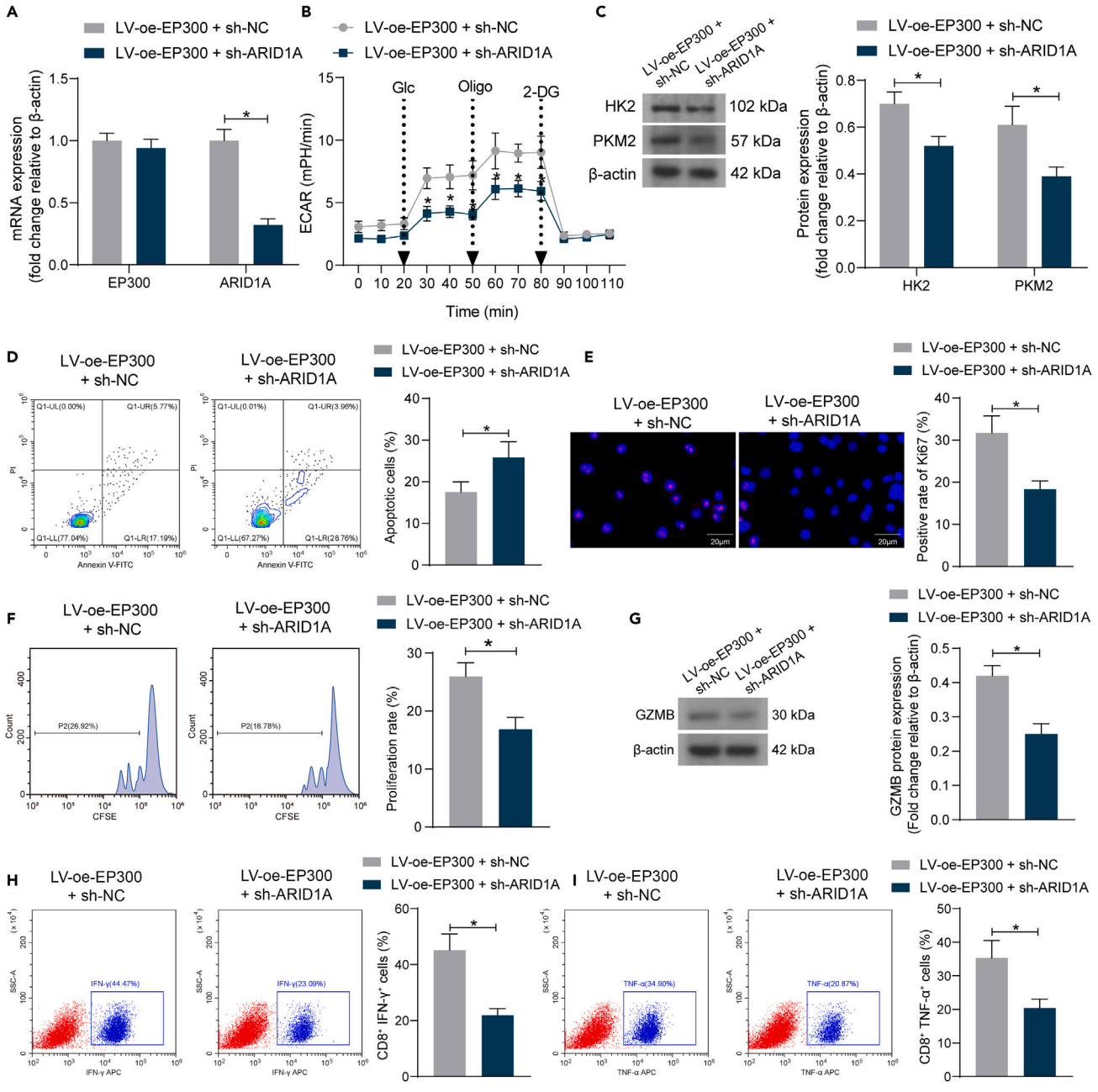

Figure 7. Knockdown of ARID1A affects the activity of CD8$^+$ T cells

(A) ARID1A mRNA expression in CD8$^+$ T cells after LV-sh-ARID1A infection in the presence of EP300 overexpression detected by qPCR analysis.

(B) ECAR of the CD8$^+$ T cells after BPTF knockdown.

(C) Protein levels of HK2 and PKM2 in CD8$^+$ T cells detected by immunoblot analysis.

(D) Apoptosis of CD8$^+$ T cells determined by flow cytometry (FITC and PI labeling).

(E) Expression of Ki67 in CD8$^+$ T cells determined by immunofluorescence staining.

(F) Proliferation of CD8$^+$ T cells determined by flow cytometry (CFSE labeling).

(G) Protein level of GZMB in CD8$^+$ T cells detected by immunoblot analysis.

(H and I) Proportions of IFN-γ^+ (H) and TNF-α^+ (I) CD8$^+$ T cells analyzed by flow cytometer.

Differences were compared by the unpaired *t* test (D–I) or two-way (A–C) ANOVA. *p < 0.05. Three biological replicates were performed. The error bar denotes the standard deviation. In panel F, scale bar = 20 μm.

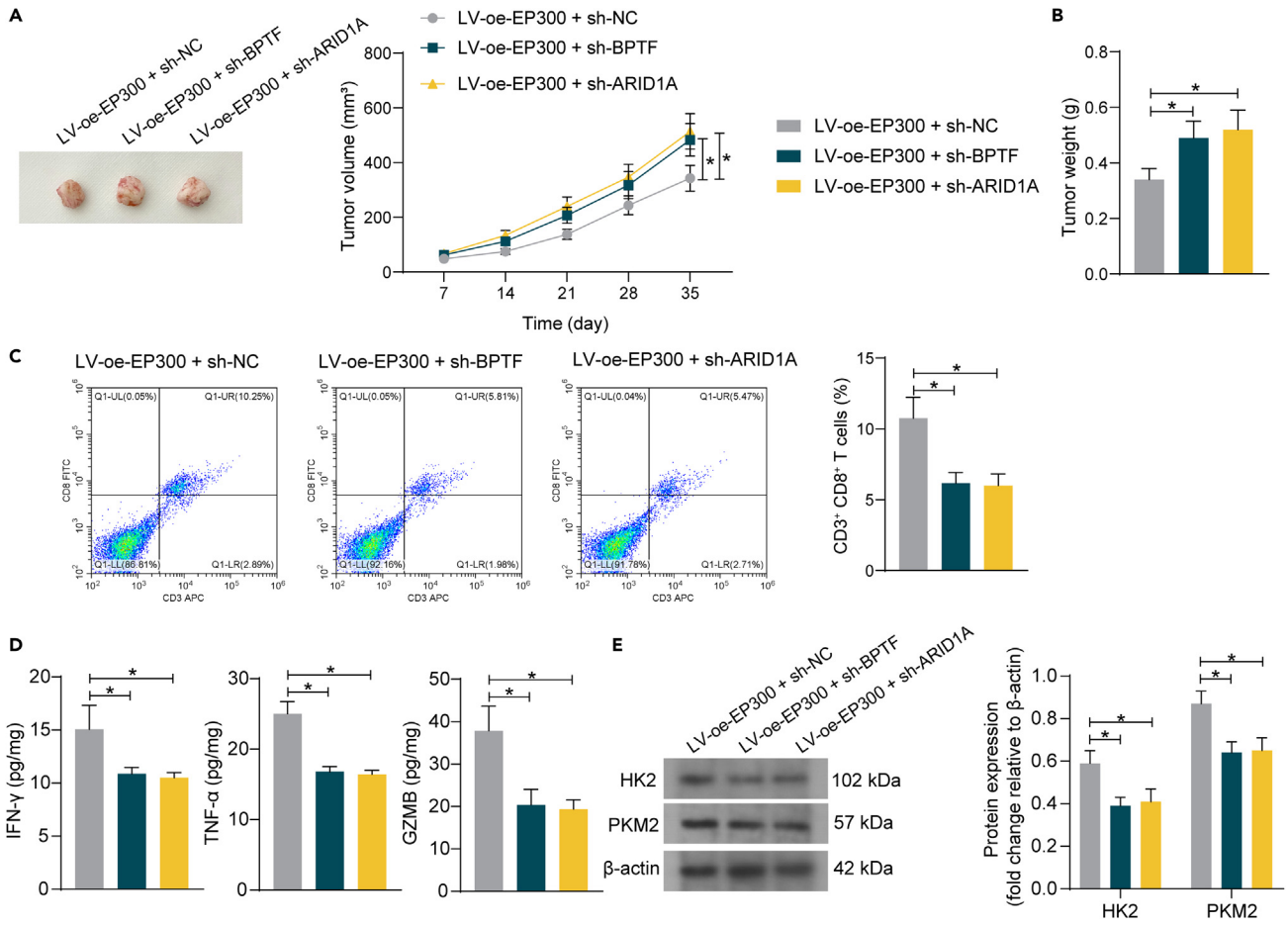

Figure 8. Knockdown of BPTF or ARID1A counteracts the effects of EP300-mediated CD8⁺ T activity *in vivo*

(A) Volume change of the xenograft tumors in mice.

(B) Tumor weight in each group of mice on day 35.

(C) Proportion of active $CD8^+$ T cells in the single cell suspension of xenograft tumor tissues analyzed by flow cytometry.

(D) Contents of IFN-γ, TNF-α, and GZMB in xenograft tumor tissues determined using ELISA kits.

(E) Protein levels of HK2 and PKM2 in the $CD8^+$ T cells sorted from tumor tissues examined by immunoblot analysis.

Differences were compared by one-way (B–D) or two-way (A and E) ANOVA. *$p < 0.05$. For animal experiments, each group contained five mice. The error bar denotes the standard deviation.

Funding: This research was supported by Doctoral Research Foundation Project of Liaoning Province (Grant No. 2022-BS-130), the Projects of Shenyang Science and Technology Bureau (grant no. 20-205-4-029) and the 345 Talent Project of Shengjing Hospital of China Medical University.

AUTHOR CONTRIBUTIONS

Zhixiu Xia: conceptualization, data curation, validation, and writing–original draft. Xiaoxu Ding: formal analysis, funding acquisition, and writing–original draft. Chao Ji: investigation, data curation, and visualization. Dabo Zhou: investigation, formal analysis, and data curation. Xun Sun: validation and writing–review and editing. Tiancong Liu: methodology, funding acquisition, software, and writing–review and editing.

DECLARATION OF INTERESTS

The authors declare no competing interests.

Received: April 4, 2023
Revised: August 30, 2023
Accepted: January 15, 2024
Published: January 17, 2024

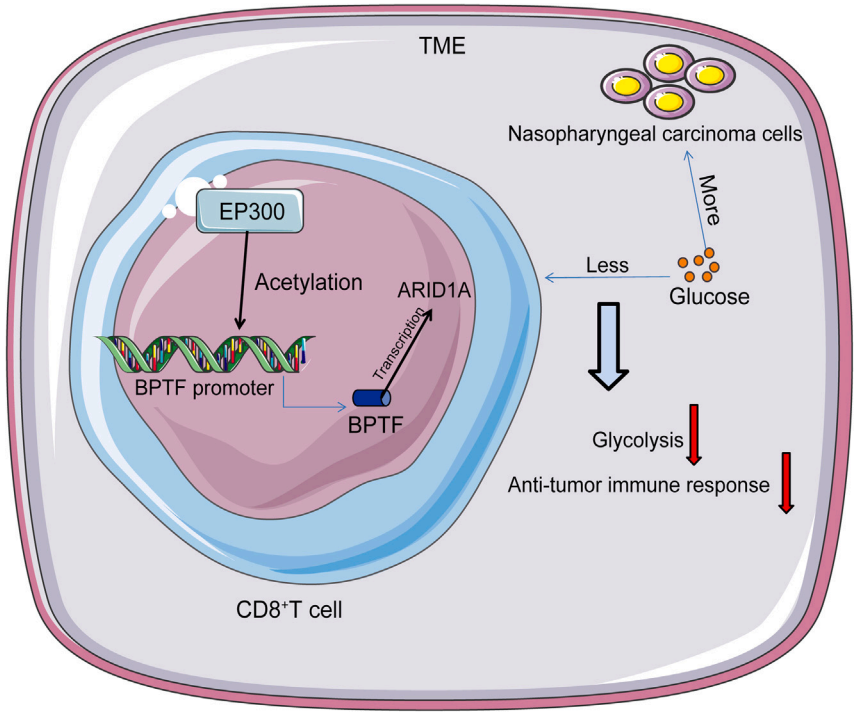

Figure 9. Graphical abstract

In the TME of NPC, the glucose glycolytic activity of $CD8^+$ T cells is reduced, leading to impaired anti-tumor effect.
EP300 upregulation increases BPTF expression through H3K27ac, and BPTF further activates transcription of ARID1A to restore the glycolytic activity and anti-tumor function of $CD8^+$ T cells.

REFERENCES

1. Duan, W., Xiong, B., Tian, T., Zou, X., He, Z., and Zhang, L. (2022). Radiomics in Nasopharyngeal Carcinoma. Clin. Med. Insights Oncol. *16*, 11795549221079186.
2. Sung, H., Ferlay, J., Siegel, R.L., Laversanne, M., Soerjomataram, I., Jemal, A., and Bray, F. (2021). Global Cancer Statistics 2020: GLOBOCAN Estimates of Incidence and Mortality Worldwide for 36 Cancers in 185 Countries. CA Cancer J. Clin. *71*, 209–249.
3. Tang, L.L., Chen, W.Q., Xue, W.Q., He, Y.Q., Zheng, R.S., Zeng, Y.X., and Jia, W.H. (2016). Global trends in incidence and mortality of nasopharyngeal carcinoma. Cancer Lett. *374*, 22–30.
4. Thommen, D.S., and Schumacher, T.N. (2018). T Cell Dysfunction in Cancer. Cancer Cell *33*, 547–562.
5. Chen, Y.P., Chan, A.T.C., Le, Q.T., Blanchard, P., Sun, Y., and Ma, J. (2019). Nasopharyngeal carcinoma. Lancet *394*, 64–80.
6. MacIver, N.J., Michalek, R.D., and Rathmell, J.C. (2013). Metabolic regulation of T lymphocytes. Annu. Rev. Immunol. *31*, 259–283.
7. Pearce, E.L., Poffenberger, M.C., Chang, C.H., and Jones, R.G. (2013). Fueling immunity: insights into metabolism and lymphocyte function. Science *342*, 1242454.
8. Liberti, M.V., and Locasale, J.W. (2016). The Warburg Effect: How Does it Benefit Cancer Cells? Trends Biochem. Sci. *41*, 211–218.
9. Qiu, J., Villa, M., Sanin, D.E., Buck, M.D., O'Sullivan, D., Ching, R., Matsushita, M., Grzes, K.M., Winkler, F., Chang, C.H., et al. (2019). Acetate Promotes T Cell Effector Function during Glucose Restriction. Cell Rep. *27*, 2063–2074.e5.
10. Yang, G., Yuan, Y., Yuan, H., Wang, J., Yun, H., Geng, Y., Zhao, M., Li, L., Weng, Y., Liu, Z., et al. (2021). Histone acetyltransferase 1 is a succinyltransferase for histones and non-histones and promotes tumorigenesis. EMBO Rep. *22*, e50967.
11. Audia, J.E., and Campbell, R.M. (2016). Histone Modifications and Cancer. Cold Spring Harb. Perspect. Biol. *8*, a019521.
12. Gayther, S.A., Batley, S.J., Linger, L., Bannister, A., Thorpe, K., Chin, S.F., Daigo, Y., Russell, P., Wilson, A., Sowter, H.M., et al. (2000). Mutations truncating the EP300 acetylase in human cancers. Nat. Genet. *24*, 300–303.
13. Kong, S., Kim, S.J., Sandal, B., Lee, S.M., Gao, B., Zhang, D.D., and Fang, D. (2011). The type III histone deacetylase Sirt1 protein suppresses p300-mediated histone H3 lysine 56 acetylation at Bclaf1 promoter to inhibit T cell activation. J. Biol. Chem. *286*, 16967–16975.
14. Liu, Y., Wang, L., Predina, J., Han, R., Beier, U.H., Wang, L.C.S., Kapoor, V., Bhatti, T.R., Akimova, T., Singhal, S., et al. (2013). Inhibition of p300 impairs Foxp3(+) T regulatory cell function and promotes antitumor immunity. Nat. Med. *19*, 1173–1177.
15. Huang, H., Tang, S., Ji, M., Tang, Z., Shimada, M., Liu, X., Qi, S., Locasale, J.W., Roeder, R.G., Zhao, Y., and Li, X. (2018). p300-Mediated Lysine 2-Hydroxyisobutyrylation Regulates Glycolysis. Mol. Cell *70*, 663–678.e6.
16. Landry, J.W., Banerjee, S., Taylor, B., Aplan, P.D., Singer, A., and Wu, C. (2011). Chromatin remodeling complex NURF regulates thymocyte maturation. Genes Dev. *25*, 275–286.
17. Yang, X., Wang, X., Lei, L., Su, Y., Zou, Y., Liu, H., Jiao, A., Zhang, C., Liu, J., Li, W., et al. (2022). Arid1a promotes thymocyte development through beta-selection-dependent and beta-selection-independent mechanisms. Immunology *165*, 402–413.
18. Gooden, M.J.M., de Bock, G.H., Leffers, N., Daemen, T., and Nijman, H.W. (2011). The prognostic influence of tumour-infiltrating lymphocytes in cancer: a systematic review with meta-analysis. Br. J. Cancer *105*, 93–103.
19. Cham, C.M., Driessens, G., O'Keefe, J.P., and Gajewski, T.F. (2008). Glucose deprivation inhibits multiple key gene expression events and effector functions in CD8+ T cells. Eur. J. Immunol. *38*, 2438–2450.
20. Sanchís, V., Marín, S., and Ramos, A.J. (2000). [Emerging mycotoxin control. Current limits and regulations]. Rev. Iberoam. De. Micol. *17*, S69–S76.
21. Jacobs, S.R., Herman, C.E., Maciver, N.J., Wofford, J.A., Wieman, H.L., Hammen, J.J., and Rathmell, J.C. (2008). Glucose uptake is limiting in T cell activation and requires CD28-mediated Akt-dependent and independent pathways. J. Immunol. *180*, 4476–4486.
22. Chang, C.H., Qiu, J., O'Sullivan, D., Buck, M.D., Noguchi, T., Curtis, J.D., Chen, Q.,

Gindin, M., Gubin, M.M., van der Windt, G.J.W., et al. (2015). Metabolic Competition in the Tumor Microenvironment Is a Driver of Cancer Progression. Cell *162*, 1229–1241.
23. Saucillo, D.C., Gerriets, V.A., Sheng, J., Rathmell, J.C., and Maciver, N.J. (2014). Leptin metabolically licenses T cells for activation to link nutrition and immunity. J. Immunol. *192*, 136–144.
24. Yang, Z., Zhang, C., Liu, X., Che, N., Feng, Y., and Xuan, Y. (2022). SETD5 Regulates Glycolysis in Breast Cancer Stem-Like Cells and Fuels Tumor Growth. Am. J. Pathol. *192*, 712–721.
25. Qi, W., Zhang, Y., Wang, Y., Wang, H., Fu, R., and Shao, Z. (2022). Abnormal expression of histone acetylases in CD8+ T cells of patients with severe aplastic anemia. J. Clin. Lab. Anal. *36*, e24339.
26. Durbin, A.D., Wang, T., Wimalasena, V.K., Zimmerman, M.W., Li, D., Dharia, N.V., Mariani, L., Shendy, N.A.M., Nance, S., Patel, A.G., et al. (2022). EP300 Selectively Controls the Enhancer Landscape of MYCN-Amplified Neuroblastoma. Cancer Discov. *12*, 730–751.
27. Wu, B., Wang, Y., Wang, C., Wang, G.G., Wu, J., and Wan, Y.Y. (2016). BPTF Is Essential for T Cell Homeostasis and Function. J. Immunol. *197*, 4325–4333.
28. Lin, J., Wang, X., Zhai, S., Shi, M., Peng, C., Deng, X., Fu, D., Wang, J., and Shen, B. (2022). Hypoxia-induced exosomal circPDK1 promotes pancreatic cancer glycolysis via c-myc activation by modulating miR-628-3p/BPTF axis and degrading BIN1. J. Hematol. Oncol. *15*, 128.
29. Zhang, C., Chen, L., Liu, Y., Huang, J., Liu, A., Xu, Y., Shen, Y., He, H., and Xu, D. (2021). Downregulated METTL14 accumulates BPTF that reinforces super-enhancers and distal lung metastasis via glycolytic reprogramming in renal cell carcinoma. Theranostics *11*, 3676–3693.
30. Astori, A., Tingvall-Gustafsson, J., Kuruvilla, J., Coyaud, E., Laurent, E.M.N., Sunnerhagen, M., Åhsberg, J., Ungerbäck, J., Strid, T., Sigvardsson, M., et al. (2020). ARID1a Associates with Lymphoid-Restricted Transcription Factors and Has an Essential Role in T Cell Development. J. Immunol. *205*, 1419–1432.
31. Jung, U.S., Min, K.W., Kim, D.H., Kwon, M.J., Park, H., and Jang, H.S. (2021). Suppression of ARID1A associated with decreased CD8 T cells improves cell survival of ovarian clear cell carcinoma. J. Gynecol. Oncol. *32*, e3.
32. Li, J., Wang, W., Zhang, Y., Cieślik, M., Guo, J., Tan, M., Green, M.D., Wang, W., Lin, H., Li, W., et al. (2020). Epigenetic driver mutations in ARID1A shape cancer immune phenotype and immunotherapy. J. Clin. Invest. *130*, 2712–2726.
33. Tang, X., Tang, Q., Mao, Y., Huang, X., Jia, L., Zhu, J., and Feng, Z. (2019). CD137 Co-Stimulation Improves The Antitumor Effect Of LMP1-Specific Chimeric Antigen Receptor T Cells In Vitro And In Vivo. OncoTargets Ther. *12*, 9341–9350.
34. Zhang, X., Wang, T., Zhu, X., Lu, Y., Li, M., Huang, Z., Han, D., Zhang, L., Wu, Y., Li, L., et al. (2023). GMP development and preclinical validation of CAR-T cells targeting a lytic EBV antigen for therapy of EBV-associated malignancies. Front. Immunol. *14*, 1103695.
35. Wang, C., Li, Y., Jia, L., Kim, J.K., Li, J., Deng, P., Zhang, W., Krebsbach, P.H., and Wang, C.Y. (2021). CD276 expression enables squamous cell carcinoma stem cells to evade immune surveillance. Cell Stem Cell *28*, 1597–1613.e7.

STAR★METHODS

KEY RESOURCES TABLE

REAGENT or RESOURCE	SOURCE	IDENTIFIER
Antibodies		
Granzyme B (D2H2F) Rabbit mAb	Cell Signaling Technology	Cat#17215; RRID: AB_2798780
Recombinant Anti-Hexokinase II antibody [EPR20839]	Abcam	Cat#ab209847; RRID: AB_2904621
PKM2 antibody	Abcam	Cat#ab85555; RRID: AB_10562282
p300 (D8Z4E) Rabbit mAb	Cell Signaling Technology	Cat#86377; RRID: AB_2800077
beta actin antibody-Loading Control	Abcam	Cat#ab8227; RRID: AB_2305186
Goat Anti-Rabbit IgG-H&L Polyclonal antibody, Hrp Conjugated	Abcam	Cat#ab6721; RRID: AB_955447
APC Anti-Interferon gamma Antibody	Abcam	Cat#ab188415; RRID: AB_2747842
APC Anti-TNF alpha Antibody	Abcam	Cat#ab269282
FITC fluorescent Anti-CD8 antibody	Abcam	Cat#ab28010; RRID: AB_726668
APC Anti-CD3 Antibody	Abcam	Cat#ab239287
APC Anti-TIM 3 Antibody	Abcam	Cat#ab155379
APC Anti-PD1 Antibody	Abcam	Cat#ab272338
Anti-Ki67 Antibody	Abcam	Cat#ab15580; RRID: AB_443209
Goat anti rabbit IgG H&L (Alexa Fluor®647) Preadsorption secondary antibody	Abcam	Cat#ab150083; RRID: AB_2714032
FALZ/BPTF Polyclonal Antibody	Thermo Fisher Scientific	Cat#A300-973A; RRID: AB_2067219
Rabbit IgG, polyclonal Antibody	Abcam	Cat#ab171870; RRID: AB_2687657
Chemicals, peptides, and recombinant proteins		
Dynabeads™ Human T-Activator CD3/CD28 for T cell Expansion and Activation	Thermo Fisher Scientific	Cat#11161D; RRID: AB_2916088
Critical commercial assays		
TransScript® Reverse Transcriptase	TransGen Biotech	Cat#AT101-02
TransStart® Green qPCR SuperMix	TransGen Biotech	Cat#AQ101-01
Human IFN-gamma DuoSet ELISA Kit	R and D Systems	Cat#DY285B; RRID: AB_2928044
TNF-alpha (human) ELISA Kit	Biovision	Cat#E4603
Granzyme B (human) ELISA Kit	Biovision	Cat#K4279
gentleMACS™ Dissociator	Miltenyi Biotec	Cat#130-093-235
Annexin V-FITC/PI Apoptosis Detection Kit	MedChemExpress	Cat#HY-K1073
Seahorse XF Glycolysis Stress Test	Agilent Technologies	Cat#103017-100
CFDA SE Cell Proliferation and Tracer Detection Kit	Beyotime	Cat#C0051
Cell Counting Kit-8 kit	Sangon Biotech	E606335
pGL3 Luciferase Reporter Vectors	Promega	Cat#E1751
Dual-Luciferase® Reporter Assay System	Promega	Cat#E1910
Experimental models: Cell lines		
Primary $CD8^+$ Cytotoxic T Cells	American Type Culture Collection	Cat#PCS-800-017
c666-1	BeNa Culture Collection	Cat#BNCC337872; RRID: CVCL_7949
Experimental models: Organisms/strains		
NOD/SCID Mice	Charles River	N/A

(*Continued on next page*)

Continued

REAGENT or RESOURCE	SOURCE	IDENTIFIER
Oligonucleotides		
qPCR primer sequences, see Table S1	This paper	N/A
Sh-BPTF sequence ATCTGTAAAACGCCTTATGATGAA TCTAAATTTTATATTGG Sh-ARID1A GGTATGGTCAACAGGGCCAGACTC CATATTACAACCAGCAA	VectorBuilder Inc	N/A
Software and algorithms		
ImageJ	Schneider et al., 2012	https://ImageJ.net/
GraphPad Prism8.0.2	GraphPad	http://www.graphpad.com/
CytoSYS1.1	BEAMDIAG Biotechnologies	N/A

RESOURCE AVAILABILITY

Lead contact

Further information and requests concerning resources and reagents should be directed to and will be answered by the lead contact, Dr. Tiancong Liu (tcliu@cmu.edu.cn).

Materials availability

This study did not generate any unique new reagent. All reagents used in this study are commercially available.

Data and code availability

(1) All data reported in this paper will be shared by the lead contact upon request.
(2) This paper does not report original code.
(3) Any additional information required to reanalyze the data reported in this paper is available from the lead contact upon request.

EXPERIMENTAL MODEL AND STUDY PARTICIPANT DETAILS

Xenograft mouse models

Forty NOD/SCID mice (6 weeks old) were procured from Charles River Laboratory Animal Technology (Beijing, China). After one week of acclimation, the mice were cultured in specific-pathogen-free grade cages with constant temperature (20°C–25°C) and humidity (40–60%) in a 12/12-h dark/light cycle. The mice were randomly assigned into 8 groups, n = 5 in each. Mice in each group were first injected with 100 μL of c666-1 cell suspension (10^6 cells) subcutaneously at the armpit site to induce xenograft tumors. After 7 days, the mice were further injected with phosphate-buffered saline (PBS) at the tumor site or injected with 100 μL of $CD8^+$ T cell suspension (5×10^6 cells/100 μL). The T cells had been activated by CD3/CD28 antibodies for 24 h, stimulated by the CM of c666-1 cells, or infected with different types of LV mentioned above. Thereafter, the tumor volume (V) was calculated every 7 days based on the major and minor axes measured using a Vernier caliper: V = (major axis × minor axis^2)/2. After 35 days, the mice were euthanized by excessive nembutal (150 mg/kg). The tumor tissues were then collected for further use. All animal experiments were performed with the approval of the Shengjing Hospital of China Medical University and adhered to the Guide for the Care and Use of Laboratory Animals (NIH Publication No. 85-23, revised 1996).

METHOD DETAILS

Cells

Primary $CD8^+$ cytotoxic T cells (PCS-800-017) were procured from American Type Culture Collection (ATCC, Manassas, VA, USA) and cultured in Roswell Park Memorial Institute (RPMI)-1640 containing 10% fetal bovine serum (FBS). A human NPC cell line c666-1 (BNCC337872) was procured from BeNa Culture Collection (Henan, China) and cultured in RPMI-1640 along with 10% FBS as well. The culture condition for all cells was 37°C with 5% CO_2. For c666-1 cells, the culture supernatant was collected after 3 days of culture and stored at −80°C. To induce metabolic impairment in $CD8^+$ T cells, the T cells were activated by CD3/CD28 antibodies (11161D, Thermo Fisher Scientific) for 24 h and then cultured in normal medium, conditioned medium (CM; 30% c666-1 culture supernatant +70% normal medium), or CM + 2 mg/mL glucose (CM + Glucose), respectively. After 24 h, the $CD8^+$ T cells were collected for subsequent use.

Lentivirus infection

Harvested $CD8^+$ T cells were resuspended and infected with LV-carried oe-EP300, sh-BPTF, sh-ARID1A, and the corresponding NC plasmids (all provided by VectorBuilder Inc., Guangzhou, Guangdong, China). After 48 h, the culture medium was refreshed. Stably infected (transfected) cells were screened using puromycin.

RNA extraction and quantification

Total RNA from T cells was extracted using the TRIzol kit (Thermo Fisher Scientific, Rockford, IL, USA) and reverse-transcribed to cDNA using the TransScript Reverse Transcriptase (TransGen Biotech, Beijing, China). The qPCR analysis was conducted using TransStart Green qPCR SuperMix (TransGen Biotech) on the ABI 7900 system. Expression values of target gens relative to the internal control (β-actin) were determined using the $2^{-\Delta\Delta Ct}$ method. The primer sequences are presented in Table S1.

Immunoblot analysis

Cells or tissues were lysed in radio-immunoprecipitation assay lysis buffer. The protein sample in the lysates was separated by gel electrophoresis and loaded onto the polyvinylidene fluoride membranes. The membranes were blocked by 5% non-fat milk for 1 h, washed, and reacted with antibodies of granzyme B (GZMB; 1:1,000, 17215, Cell Signaling Technology [CST], Beverly, MA, USA), hexokinase 2 (HK2; 1:1,000, ab209847, Abcam Inc., Cambridge, MA, USA), pyruvate kinase M2 (PKM2; 1:1,000, ab85555, Abcam), EP300 (1:1,000, 86377, CST) and β-actin (1:1,000, ab8227, Abcam) overnight at 4°C. Later, the membranes were further incubated with goat anti-rabbit IgG (1:2,000, ab6721, Abcam) at room temperature for 1 h. The protein bands were visualized by enhanced chemiluminescence, and the optical density of target protein bands relative to that of the internal control band (β-actin) was analyzed by ImageJ to evaluate protein expression.

Co-culture of T cells with C666-1 cells

To examine the direct cytotoxicity of T cells to NPC cells, the differentially treated activated T cells were directly co-cultured with C666-1 cells in single wells in six-well plates at an E:T ratio (effector cells: target cells) at 10:1.[35] The co-culture condition was maintained at 37°C with 5% CO_2. After 10 h, the C666-1 cells were harvested, and the cell viability and apoptosis were determined by cell counting kit-8 (CCK-8) method and flow cytometry, respectively.

CCK-8 method

Viability of C666-1 cells after co-culture with T cells was analyzed using the CCK-8 kit (E606335, Sangon Biotech Co., Ltd., Shanghai, China). In short, the cells were seeded in 96-well plates, followed by incubation with 10 μL CCK-8 solution at 37°C with 5% CO_2 for 2 h. The optical density at 450 nm was determined.

Enzyme-linked immunosorbent assay (ELISA)

The xenograft tumor tissues were made into homogenate, in which the contents of IFN-γ, TNF-α, and GZMB were determined using the human IFN-gamma DuoSet ELISA kit (DY285B, R&D Systems, Minneapolis, MN, USA), the human TNF-alpha ELISA kit (E4603, BioVision, Milpitas, CA, USA), and the human Granzyme B ELISA kit (K4279, BioVision) according to the manufacturers' protocols.

Flow cytometry

Mouse tumor tissues were cut into sections and soaked in RPMI-1640 containing collagenase and DNase I, and then dissociated into cell suspension using the MACS Dissociator (Miltenyi Biotec, Auburn, CA, USA). After 1 h of incubation, the cells were filtered to obtain single cell suspension. The proportion of activated $CD8^+$ T cells was screened by the Attune NxT flow cytometer (Thermo Fisher Scientific) using the antibodies of allophycocyanin (APC)-CD3 (ab239287, Abcam), fluorescein isothiocyanate (FITC)-CD8 (ab28010, Abcam), APC-TIM-3 (ab155379, Abcam), APC-PD-1 (ab272338, Abcam) at 4°C overnight.

Apoptosis of $CD8^+$ T cells and C666-1 cells after co-culture with T cells was analyzed using the Annexin V-FITC/propidium iodide (PI) Apoptosis Detection Kit (HY-K1073, MedChemExpress, Monmouth Junction, NJ, USA). In short, the treated $CD8^+$ T cells were digested and resuspended, and then reacted with 5 μL Annexin V-FITC and 10 μL PI in the dark for 20 min. The apoptosis of cells was analyzed using the Attune NxT flow cytometer.

The cytotoxicity of $CD8^+$ T cells cultured *in vitro* was analyzed as well. In short, the treated $CD8^+$ T cells were digested and made into single cell suspension, followed by centrifugation and the removal of supernatant. The cell pellets were resuspended. For the detection of intracellular antigens, the cells were fixed with 4% paraformaldehyde at room temperature for 15 min, washed with PBS, and permeabilized using 0.3% Triton X-100. Following this, the cells were washed, resuspended, and then incubated with APC-IFN-γ (ab188415, Abcam) and APC-TNF-α (ab269282, Abcam) at 4°C for 30 min, followed by detection using the Attune NxT flow cytometer.

To make the flow cytometry results as accurate as possible, automatic compensation adjustments were performed during the analyzing process. For single staining, compensation was adjusted to eliminate the interference of cells' spontaneous fluorescence. For dual staining using two types of antibodies, compensation was automatically adjusted based on the fluorescent wavelengths of the fluorochromes, aiming to eliminate interference from overlapping wavelengths between cells' spontaneous fluorescence and multiple fluorochromes.

ECAR examination

The ECAR of $CD8^+$ T cells was analyzed using the Seahorse XF Glycolysis Stress Test Kit (103017-100, Agilent Technologies, Palo Alto, CA, USA). In short, the treated $CD8^+$ T cells were cultured in 8-well plates for 1 h to analyze the basal metabolism, followed by the addition of 10 nM glucose, 1 μM oligomycin and 50 mM 2-deoxyglucose (2-DG) to analyze the ECAR, as expressed as mPH/min.

Immunofluorescence staining

The treated $CD8^+$ T cells were fixed with paraformaldehyde, incubated with 0.1% Triton X-100 for 5 min, blocked with 1% bovine serum albumin for 30 min, and then incubated with the Ki67 antibody (1:1,000, ab15580, Abcam) at room temperature for 2 h. After that, the cells were incubated with Alexa Fluor 647 conjugated goat anti-rabbit (1:200, ab150083, Abcam) at room temperature for 1 h. DAPI was used for nuclear staining. The cell slides were then sealed by anti-quenching reagent and observed under the fluorescence microscopy. The positive staining rate was calculated.

$CD8^+$ T cell proliferation examined using carboxyfluorescein diacetate succinimidyl ester (CFSE) staining

The treated $CD8^+$ T cells were adjusted to 1×10^6 cells/mL. According to the instructions of the cell proliferation assay and tracking kit (C0051, Beyotime), approximately 1×10^6 cells were resuspended in 1 mL CFSE labeling solution, followed by incubation with diluted CFSE storage reagent at 37°C for 5 min. Subsequently, complete cell culture medium was added and fully mixed. The mixture was then centrifuged at room temperature to remove the supernatant. Following this, the cells were washed with complete medium and incubated at 37°C for 5 min, followed by another centrifugation and washing. Afterward, the $CD8^+$ T cells were incubated for 72 h, and then the percentage of passage 2 proliferative cells was calculated by flow cytometry.

ChIP-qPCR

The $CD8^+$ T cells were soaked in 1% formaldehyde for 10 min of protein-DNA crosslinking, and the genomic DNA was truncated by ultrasonication. The chromatin segments were reacted with specific antibodies of EP300 (1:50, 86377, CST), BPTF (1:100, A300-973A, CST) or IgG (1:1,000, ab171870, Abcam) for immunoprecipitation. The precipitated DNA was extracted and purified, and the abundance of BPTF or ARID1A promoter fragments was analyzed by qPCR analysis. Following is the information of the promoter sequences: BPTF promoter (Left) 5'-GAGGAGGAGGAAGAGGAGGA-3', BPTF promoter (Right) 5'-GTCGTCGTCTTCCATCTCCT-3'; ARID1A promoter (Left) 5'-GCCCT CGGAGCTGAAGAAA-3', BPTF promoter (Right) 5'-CGGCTGCCTTCATTTCCC-3'.

Dual luciferase reporter gene assay

The $CD8^+$ T cells were infected with LV-sh-BPTF or the corresponding NC. After 24 h, the pGL3-basic luciferase reporter vectors (E1751, Promega Corporation, Madison, WI, USA) containing the amplified ARID1A promoter sequences were further transfected into cells. The luciferase activity in cells was analyzed using the Dual-Luciferase Reporter Assay System (Promega).

QUANTIFICATION AND STATISTICAL ANALYSIS

GraphPad Prism (version 8.0.2) was used for data analysis (GraphPad, La Jolla, CA, USA). Differences among multiple groups were analyzed by one- or two-way analysis of variance (ANOVA) and Bonferroni correction. Differences between two groups were determined by two-tailed unpaired *t* test. All data are expressed as the mean ± standard deviation. The animal number for each experiment, or the repetition number of independent experiments, as well as the specific statistical methods have been clarified in figure legends.